Notation

$N :=$ number of points sampled
- $N \sim h^{-2}$
- $B :=$ number of basis functions used in vergini method
- $k :=$ wavenumber
- $E = k^2 :=$ energy of eigenfunction
- $h :=$ orthogonal spacing between sampled points
- $\alpha := kh$
- $\Omega \in \mathbb{R}^2$ compact domain
- $\Gamma = \partial\Omega$ domain boundary

Chapter 1

Introduction

1.1 Motivation

Nodal domains characterize regions of a vibrational surface (e.g. a drum head) that move together. The boundaries between nodal domains, known as nodal line are the regions which do not vibrate at all (Fig. 1.1). Understanding the characteristics of nodal domains has potential applications in musical instruments, mechanical engineering, geophysics, astrophysics, and many other areas dealing with wave behavior [9].

The nodal domains studied herein are formulated in terms of quantum mechanical wave functions on Euclidean billiards, a canonical example of quantum chaos. Quantum chaos lies at the intersection of quantum mechanics and chaos theory. The primary signature of chaos in classical systems is a nonlinear (exponential) divergence of paths in the phase space of a system. Quantum mechanics however, is entirely linear and quantum chaos deals with energy eigenfunctions of systems, which are constant in time. Thus chaos in quantum systems is manifest in different ways, one of the most studied being wavefunctions in chaotic domains. Figure 1.2 shows a classical orbit and a quantum eigenfunction on the same billiard.

The goal of this project is to numerically test certain conjectures regarding properties of nodal domains in quantum chaotic eigenfunctions in the high energy, or semiclassical, limit. Efficiently testing these conjectures requires solving new computational challenges. We hope these results will enable further mathematical investigation of eigenfunctions and that the tools developed herein may be applied to related problems in experimental mathematics.

1.2 Classical Chaos in Billiards

A billiard is a compact domain $\Omega \subset \mathbb{R}^2$. A billiard defines a map $f(\mathbf{x}, t) : \Omega \times S^1 \times \mathbb{R} \to \Omega \times S^1$ where S^1 is the unit circle and $\mathbf{x} = (q, p) \in \Omega \times S^1$ is a point in phase space where $q \in \Omega$ is a position and $p \in S^1$ is a momentum, or

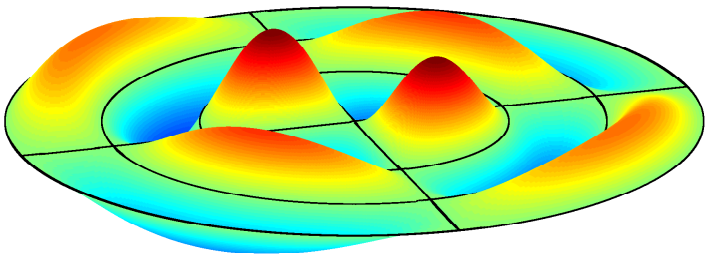

Figure 1.1: A circular vibrational surface with nodal lines shown in black. Nodal domains are regions between black lines

direction of motion. This map describes the motion of a ball bouncing in the domain Ω.

Chaos in classical systems is characterized by the Lyapunov exponent λ of a system, which describes how quickly nearby trajectories diverge. It is computed as the long time ratio of the divergence of two initially close paths:

$$\lambda = \lim_{t\to\infty} \lim_{|\boldsymbol{\epsilon}|\to 0} \frac{1}{t} \frac{|f(\mathbf{x_0}, t) - f(\mathbf{x_0} + \boldsymbol{\epsilon}, t)|}{|\boldsymbol{\epsilon}|}$$

From this definition it follows that

$$|f(\mathbf{x_0}, t) - f(\mathbf{x_0} + \boldsymbol{\epsilon}, t)| \approx e^{\lambda t} |\boldsymbol{\epsilon}|$$

for small $\boldsymbol{\epsilon}$ and large t. Thus a tiny change $\boldsymbol{\epsilon}$ in initial conditions produces a change that grows exponentially over time with growth rate λ. Chaotic systems have a positive Lyapunov exponent and therefore have unpredictable long-term behavior because arbitrarily small errors in measurements of initial conditions eventually become large. As these errors grow to the size of the domain, the position of a particle approaches a uniform distribution over the entire billiard. The property that small subsets of Ω eventually map to all of Ω is known as ergodicity (see appendix A for a formal definition).

1.3 Quantum Chaos in Billiards

A quantum wave-particle in a billiard Ω obeys the Schrödinger equation

$$Eu(\mathbf{r}) = -\frac{\hbar^2}{2m} \Delta u(\mathbf{r}) + V(\mathbf{r}) u(\mathbf{r})$$

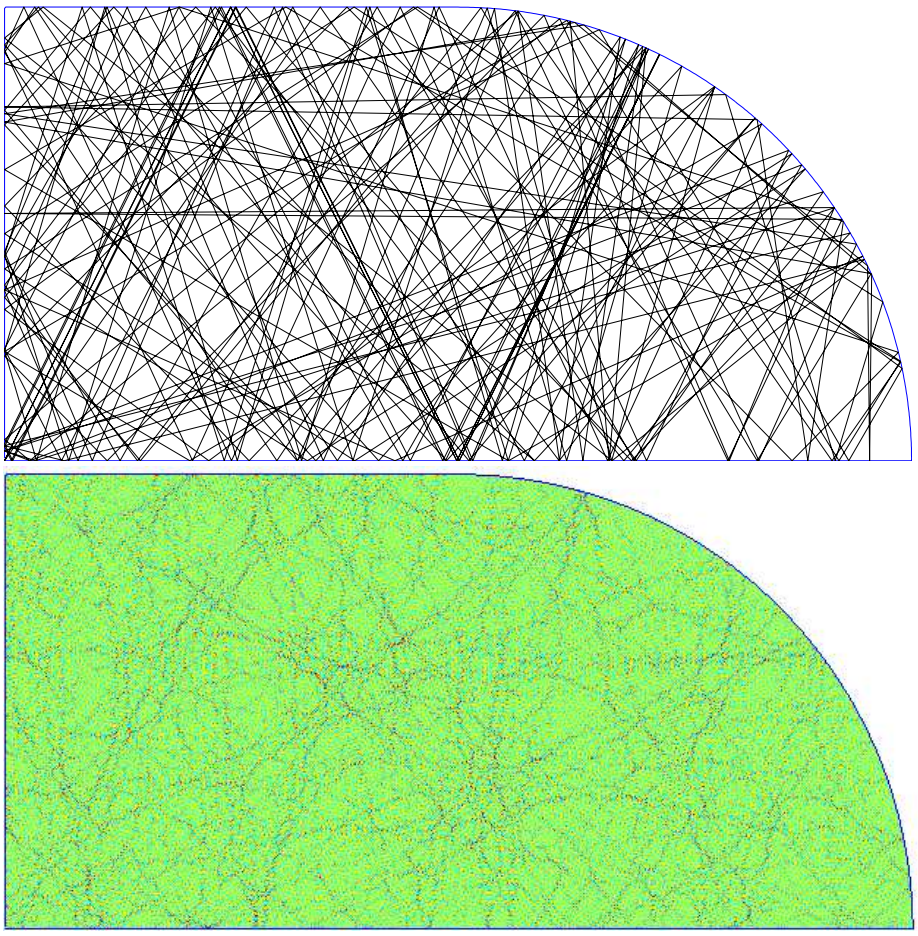

Figure 1.2: Top: A classical orbit in a billiard; bottom: a quantum eigenfunction in the same billiard

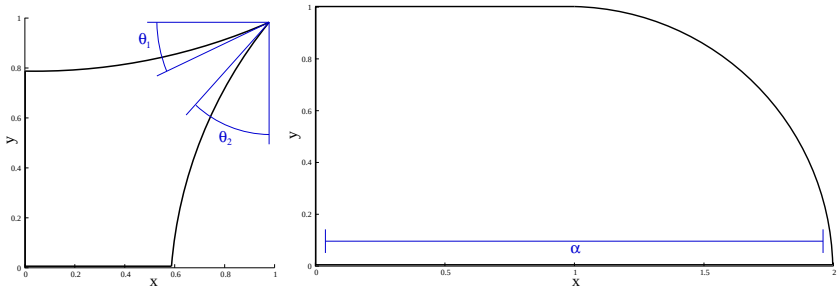

Figure 1.3: Left: quarter generalized rectangular Sinai billiard; right: quarter stadium billiard

Where $\Delta = \nabla^2 = \frac{\partial^2}{\partial x^2} + \frac{\partial^2}{\partial y^2}$ is the Laplacian differential operator in two dimensions. Setting $\hbar = 2m = 1$ and $V(\mathbf{r}) = 0$ for $\mathbf{r} \in \Omega$ while enforcing Dirichlet boundary conditions $u(\mathbf{r}) = 0$ for $\mathbf{r} \in \Gamma = \partial\Omega$ simplifies this to the Helmholtz equation

$$\begin{cases} (\Delta + k^2)u(\mathbf{r}) = 0 & \text{if } \mathbf{r} \in \Omega \\ u(\mathbf{r}) = 0 & \text{if } \mathbf{r} \in \Gamma \end{cases} \tag{1.1}$$

where $k^2 = E$ is the energy of the eigenfunction $u(\mathbf{r})$ and corresponds to the kinetic energy of the quantum wave-particle.

We focus our investigation on two billard shapes: the generalized rectangular Sinai billiard and the Stadium billiard. In both cases we desymmetrize the billard shapes by considering only a quarter of the full shape. This restricts our basis set to functions that are odd as a function of x and y, i.e., $f(-x, y) = f(x, -y) = -f(x, y)$. The desymmetrized billiards are shown in figure 1.3

The Sinai billiard is constructed from circular arcs that meet at $(1, 1)$ and is parameterized by two angles, θ_1 and θ_2, the angles from horizonal and vertical, respectively, of the arcs at $(1, 1)$. The Sinai billiard is said to demonstrate "hard chaos" becase there are no stable orbits.

The stadium billiard is construced from a rectangular region and a quarter circle and is parameterized by the the horizontal length of the billiard α. The stadium billiard contians neutrally stable orbits, specifically those with vertical momentum in the rectangular region. Neutrally stable orbits have zero Lyapunov exponent but any perturbation will cause them to have positive Lyapunov exponenet. The existence of such orbits implies that the stadium does not demonstrate hard chaos but because these orbits occupy a measure zero subset of phase space, the stadium still demonstrates chaotic properties.

1.4 Percolation Model

Bogomolny and Schmit [4] have argued that nodal domains of random functions (which are considered an accurate proxy for eigenfunctions of chaotic systems)

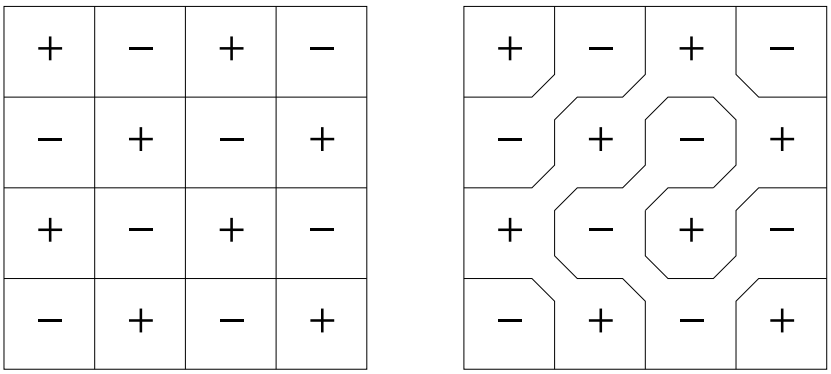

Figure 1.4: Left: checkerboard pattern; right: perturbed checkerboard pattern

can be modeled by nodal domains of a percolation model. Their percolation model is formed by creating a checkerboard of positive and negative regions with a grid size given by the average spacing of zeros of random functions along a particular axis. This checkerboard pattern can be realized as an eigenfunction $\bar{u}(x,y) = sin(\frac{kx}{\sqrt{2}})sin(\frac{ky}{\sqrt{2}})$ of a square billiard $\Omega = [0,1]^2$. A random eigenfunction can be modelled as this mean eigenfunction $\bar{u}(x,y)$ plus another term representing deviation from the mean $u(x,y) = \bar{u}(x,y) + \delta u(x,y)$. The deviation term $\delta u(x,y)$ is modelled by perturbing each nodal line crossing by connecting two diagonal regions (Fig. 1.4). The decision of which nodal domains to connect is made randomly with equal probability for either possibility.

Bogomolny and Schmit apply results from graph theory and statistical physics to compute the distribution of nodal domains in this percolation model. These results form the two primary conjectures we wish to test numerically.

Conjecture 1 (Mean of Nodal Domain Count)**.** *The number of nodal domains $\nu(E)$ in a quantum chaotic eigenfunction with energy E is normally distributed with mean*

$$\frac{\bar{\nu}(E)}{\bar{N}(E)} = \frac{3\sqrt{3}-5}{\pi} \approx 0.0624 \tag{1.2}$$

Conjecture 2 (Variance of Nodal Domain Count)**.** *The number of nodal domains $\nu(E)$ in a quantum chaotic eigenfunction with energy E is normally distributed with variance*

$$\frac{\sigma^2(\nu(E))}{\bar{N}(E)} = \frac{18}{\pi^2} + \frac{4\sqrt{3}}{\pi} - \frac{25}{2\pi} \approx 0.0502 \tag{1.3}$$

In both conjectures, $\bar{N}(E)$ is the mean number of eigenfunctions with energy less than E which is given by Weyl's law [5] to be

$$\bar{N}(E) = \frac{|\Omega|E}{4\pi}$$

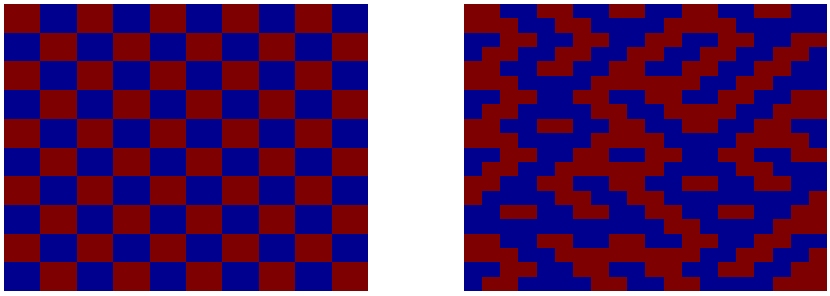

Figure 1.5: Left: checkerboard pattern implementation; right: perturbed checkerboard pattern implementation

Bogolmony and Schmit also obtain a prediction for the distribution of areas of nodal domains

Conjecture 3 (Area of Nodal Domains)**.** *The area s of nodal domains in a quantum chaotic eigenfunction follows the distribution*

$$f(s) \propto s^{-\tau} \tag{1.4}$$

where $\tau = \frac{187}{91}$ is the Fisher exponent.

1.4.1 Implementation

The percolation model was implemented in code by creating a checkerboard pattern with each square being two pixels by two pixel that was then perturbed at each nodal line crossing by changing the sign of a pixel to either connect the top right square to the bottom left square or the top left square to the bottom right square 1.5. The number of squares in the grid m is determined by k to be [4].

$$m = \frac{k}{\sqrt{2}\pi}$$

Making each square two pixels by two pixels uses a grid of size $\frac{2k^2}{\pi^2}$ on which the nodal domain counting algorithm described in 2.2 can be used.

Chapter 2

Methods

2.1 Scaling Method

2.1.1 Theory

Vergini and Saraceno [8] developed a method of computing high energy eigenfunctions of chaotic billiards using a scaling method. The method simultaneously finds all eigenfunctions $\phi_i(\mathbf{r})$ with wavenumber in a given window $[k - \Delta k, k + \Delta k]$ by scaling each eigenfunction. The scaled eigenfunctions $\chi_i(k, \mathbf{r})$ are computed as

$$\chi_i(k, \mathbf{r}) = \phi_i\left(\frac{k}{k_i}\mathbf{r}\right) = \phi_i\left(\mathbf{r} + \frac{\omega_i}{k_i}\mathbf{r}\right)$$

where $\omega_i = k - k_i$. This scaling causes all eigenfunctions to fall approximately in a linear subspace of a single basis set $\{\xi_l\}_{l=1}^{B}$, that is

$$\chi_i(k, \mathbf{r}) = \sum_{l=1}^{B} X_{li}\xi_l(k, \mathbf{r}) + \epsilon_i(\mathbf{r})$$

where $\epsilon_i(\mathbf{r}) \ll 1$ for sufficiently large B, the number of basis functions used. Values of B of approximately $1.5\frac{k|\Gamma|}{\pi}$ have been shown to produce $\epsilon < 10^{-4}$. This single basis set provides a significant efficiency gain over prior methods because many eigenfunctions can be found by solving a single linear system and evaluating a single basis set on the domain.

The choice of basis functions $\xi_l(k, \mathbf{r})$ depend on the billiard shape being used. For the quarter generalized rectangular Sinai billiard the basis set consists of irregular Bessel functions (which satisfy $(\Delta + k^2)\xi_l(k, \mathbf{r}) = 0$) placed along Γ^+, the set of points ouside Ω whose nearest distance to Γ is D where kD is taken to be 7 so that D is appriximately one wavelength. For the quarter stadium, the basis set is plane waves with orientations evently spaced around the circle. The scaling method runs in $O(B^3) = O(k^3)$ time. [2]

Billiard	Ratio	k_c
Sinai	75	3860
Stadium	31	550

Table 2.1: Ratios of basis function evaluation time to coefficient multiplication time for various billiards. Column k_c contains the value of k for which n is equal to the given ratio with $\Delta k = 0.1$ and coefficient multiplications take as long as evaluating basis functions

2.1.2 Run Time

The scaling method only computes coefficients of basis functions, which must be evaluated in order to obtain eigenfunction values at arbitrary $\mathbf{r} \in \Omega$. However, because all eigenfunctions in the energy window use the same basis functions, each basis function only needs to be evaluated once at each point, regardless of the number n of eigenfunctions in the energy window. Thus NB basis function evaluations are required. Computing eigenfunctions is then just a matter of multiplying the basis function values at each point by the coefficients for that eigenfunction, which requires a total of nNB multiplications. Basis evaluation are much more expensive than multiplications however. Table 2.1 summarizes the ratios of these costs.

Errors in eigenfunctions produced by the scaling method scale like $O(\Delta E^3)$ [3] and are independent of E so we use a constant ΔE. We estimate errors by calculating the tension

$$t = \left(\int_\Gamma u(\mathbf{r})^2 d\mathbf{r} \right)^{\frac{1}{2}}$$

ΔE is chosen such that $t \lesssim 10^{-4}$. Using Weyl's law we can obtain an estimate of the number of eigenfunctions in an energy window to be

$$n \approx \frac{|\Omega|}{4\pi}((k+\Delta k)^2 - (k-\Delta k)^2) = \frac{|\Omega|}{\pi} k \Delta k$$

where $k = \sqrt{E}$ and $2k\Delta k = \Delta E$.

We choose ΔE to be as large as possible while keeping errors small in order to maximize n, allowing more eigenfunctions to be computed from each evaluation of basis functions.

For both billiards considered here $B \sim k$. Thus, in practice $N \gg n$ and $N \gg B$ so it is primarily N (which scales like α^{-2}) that determines the time to compute eigenfunctions. Computation time is dominated by eigenfunction evaluation, which is dominated by basis function evaluations Additionally, we find that the time to evaluate eigenfunctions dominates total computation time (Fig. 2.1).

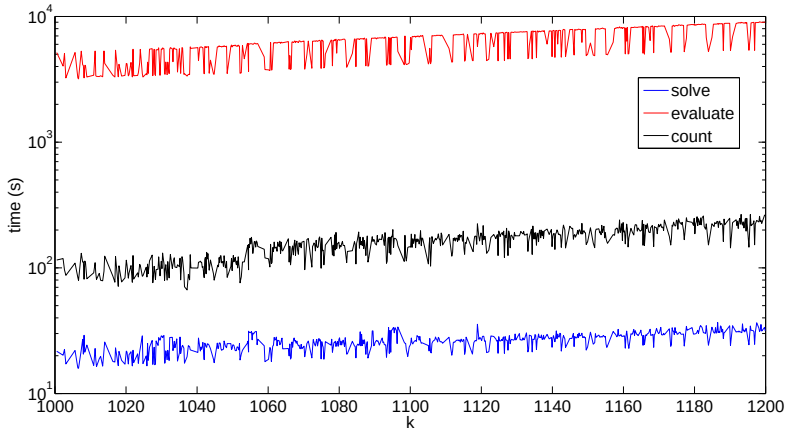

Figure 2.1: Comparison of run times at $\alpha = 0.5$ of solving for basis coefficients, evaluating eigenfunctions, and counting nodal domains. Evaluating eigenfunctions dominates runtime, taking approximately 97% of computation time.

2.2 Counting Nodal Domains

Eigenfunctions are sampled on a regular grid; each point in this grid will be referred to as a "pixel." Nodal domains are counted by exploring domains pixel-by-pixel, marking each pixel as "counted" once it has been seen. The searching algorithm usded to explore each domain is a hybrid depth- and breadth-first method where for each pixel, the sign of each neighboring pixel is compared to the sign of the nodal domain and if the sign matches, the neighboring pixel is pushed onto a stack. Exploration then continues by popping a pixel off of the stack. This method was chosen so that the signs of all four neighbors (above, below, right, and left) are known when that pixel is being examined, which is necessary for the adaptive interpolation scheme described below.

Algorithm 1 Nodal domain counting algorithm

Require: $grid$ is ny by nx matrix containing eigenfunction values on billiard
Require: $\alpha = kh$, M is highest order Bessel function to interpolate with, ρ is ratio to interpolate by

```
function CountNodalDomains(grid, α, M, ρ)
    for i ∈ 1...ny do
        for j ∈ 1...nx do
            counted[i][j] ← UNCOUNTED
        end for
    end for
    interp ← CreateInterpMatrix(α, M, ρ)
    i, j, domains ← 0
    while i, j ← FindNextUnseen(counted, i, j) do
        domains ← domains + 1
        FindDomain(grid, counted, i, j, domain_num, interp)
    end while
return domains
end function

function FindNextUnseen(counted, y, x)
    for i ∈ y...ny do
        for j ∈ 1...nx do
            if i = y and j ≤ x then
                continue
            end if
            if counted[i][j] = UNCOUNTED then
                return i, j
            end if
        end for
    end for
    return NULL
end function
```

Algorithm 1 Nodal domain counting algorithm (continued)

```
function FindDomain(grid, counted, i, j, interp)
    s.push(j, i)                                              ▷ s is a stack
    while x, y ← s.pop() do
        sign ← sign(grid[y][x])
        if InGrid(x − 1, y) then
            if sign(grid(x − 1, y)) = sign then
                left ← TRUE
                if counted[x − 1][y] = UNCOUNTED then
                    s.push(x − 1, y)
                end if
            end if
        end if
        ...                                  ▷ Same for above, right, and below
        if InGrid(x − 1, y − 1) and above and left then
            if sign(grid(x − 1, y − 1)) = sign then
                if not IsInterpolated(counted, x − 1, y − 1) then
                    Interpolate(grid, counted, x − 1, y − 1, interp)
                end if
                if ConnectedAboveLeft(counted, x, y) then s.push(x−1, y−1)
                end if
            end if
        end if
        ... ▷ Same for below and left, below and right, and above and right
        counted[y][x] = COUNTED
    end while
end function
```

Letting N be the number of points the eigenfunction is sampled at, this method has computational complexity $O(N)$. This is because the method performs a fixed number of comparisons for each pixel plus $O(N)$ total comparisons searching for an unseen nodal domain after a nodal domain has been explored. This algorithm uses an array of N integers to store, for each pixel, whether it has been counted, which nodal domain it is in, whether or not it is within the boundary of the billiard, and additional information relating to the interpolation method described below. In addition, this method uses a dynamically sized array as a stack whose size is (loosely) bounded above by the number of pixels in the nodal domain being explored.

2.3 Interpolation

Because sampling eigenfunctions is expensive (requiring evaluation of B = O(k) basis functions), we are limited by the total number of pixels N, which scales like h^{-2} where h is the distance between adjacent sample points, or the width (and

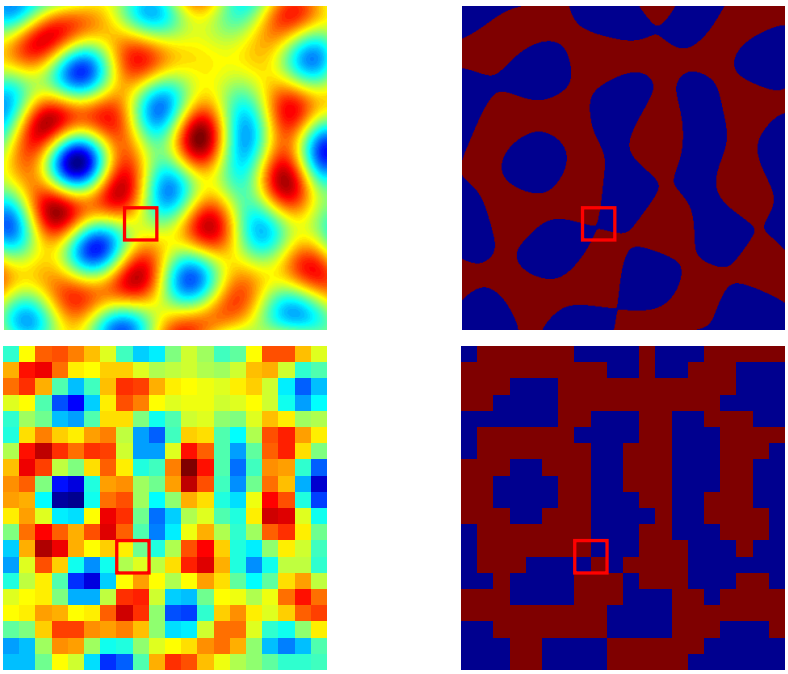

Figure 2.2: An ambiguity in nodal domain connectivity due to coarse sampling. The ambiguous region is shown with a red box. Top left: high resolution image of an eigenfunction; top right: nodal domains of the same eigenfunction; bottom left: low resolution image of the same eigenfunction; bottom right: nodal domains of low resolution eigenfunction

height) of a pixel. As a consequence, we must work with relatively coarsely sampled eigenfunctions, causing us to encounter scenarios where the connectivity of nodal domains is ambiguous (Fig. 2.2).

We resolve such ambiguities by performing an interpolation in the ambiguous region. We interpolate with the functions

$$J_n(kr)\sin(n\theta)$$

and

$$J_n(kr)\cos(n\theta)$$

where $J_n(r)$ is a regular Bessel function. These functions form a complete orthonormal basis for solutions of (1.1) (see appendix B). We fix a value M to be the order of the highest order Bessel function, restricting our basis to the

finite set

$$\xi_i(r,\theta) = \begin{cases} J_i(kr) & \text{if } i = 0 \\ J_i(kr)\sin(i\theta) & \text{if } 1 \le i \le M \\ J_{i-M}(kr)\cos((i-M)\theta) & \text{if } M+1 \le i \le 2M \end{cases} \tag{2.1}$$

We construct a surrogate function

$$\tilde{u}(\mathbf{r}) = \sum_{i=0}^{2M} c_i \xi_i(\mathbf{r})$$

as a local approximation to the eigenfunction $u(\mathbf{r})$ by fitting the coeffiecients $c_i \in \mathbb{R}$ to minimize the error $\|u - \tilde{u}\|_2$. This function can then be sampled at a higher resolution within the region in question. We define the sampling ratio of this surrogate function to the original eigenfunction to be ρ.

Chapter 3

Parameter Selection

Interpolation occurs only between the central four pixels but uses surrounding values to fit the coefficients c_i. The selection of which surrounding values to use is termed a stencil. Only stencil shapes that which are symmetric about the four central points were considered. The four shapes considered are shown in figure 3.1. The most important consideration in choosing a stencil was the accuracy of the interpolation. The size of the stencil affects the computational cost of interpolation but this difference is trivial.

The accuracy of interpolation also depends on M and $\alpha = kh$, which must be considered simultaneously with the choice of stencil. Figure 3.2 shows a comparison of the infinity norm of the interpolation error over various values of M and α for each of the stencils shown above.

Based on these data, we chose to use the 24-point stencil with $M = 9$ and $alpha \in [0.5, 0.7]$ for interpolation. For this choice of parameters we expect errors in interpolated eigenfunction values of order 10^{-6} Figure 3.3 shows the error in nodal domain counts for random plane waves with and without interpolation using these parameters.

3.0.1 Numerical Implementation

We construct a matrix to transform values on a stencil to interpolated values in the center of the stencil, performing the process described above with a single matrix multiplication. We construct the interpolation matrix as

$$U = LH^{+}$$

Where L is a matrix which contains evaluations of Bessel functions at low resolution, H contains evalutions of Bessel functions at high resolution and $^{+}$ denotes the pseudoinverse. Specifically,

$$L_{ij} = \begin{cases} J_j(r_i) & \text{for } j = 0 \text{ and } 0 \leq i < T \\ J_j(r_i)\sin(j\theta_i) & \text{for } 1 \leq j \leq M \text{ and } 0 \leq i < T \\ J_{j-M}(r_i)\cos((j-M)\theta_i) & \text{for } M+1 \leq j \leq 2M+1 \text{ and } 0 \leq i < T \end{cases}$$

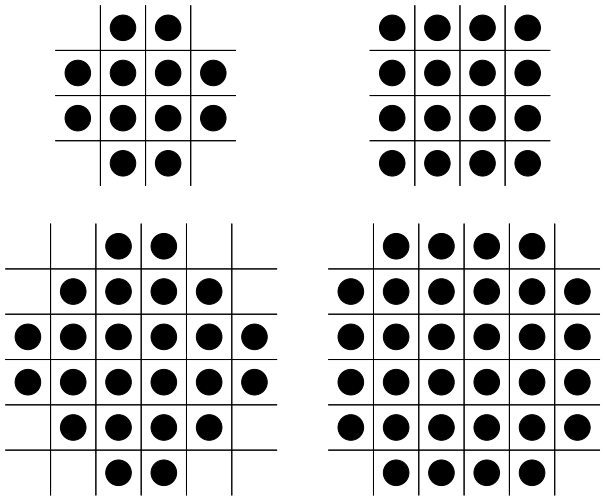

Figure 3.1: The four stencil shapes considered for interpolation

and

$$H_{ij} = \begin{cases} J_j(\tilde{r}_i) & \text{for } j = 0 \text{ and } 0 \leq i < \gamma \\ J_j(\tilde{r}_i)\sin(j\tilde{\theta}_i) & \text{for } 1 \leq j \leq M \text{ and } 0 \leq i < \gamma \\ J_{j-M}(\tilde{r}_i)\cos((j-M)\tilde{\theta}_i) & \text{for } M+1 \leq j \leq 2M+1 \text{ and } 0 \leq i < \gamma \end{cases}$$

where T is the number of points in the stencil, $\gamma = (\rho+1)^2$ and (r_i, θ_i) and $(\tilde{r}_i, \tilde{\theta}_i)$ are points in the stencil and inner square, respectively, expressed in polar coordinates.

The pseudoinverse H^+ is computed using a singular value decomposition as follows,

$$H^+ = V\Sigma^+U^*$$

where $H = U^*\Sigma V$ is a singular value decompostion of H and

$$\Sigma^+_{ii} = \begin{cases} \Sigma^{-1}_{ii} & \text{if } \Sigma_{ii} > \epsilon \\ \Sigma_{ii} & \text{otherwise} \end{cases}$$

where $\epsilon = \gamma\epsilon_{double}\Sigma_{11}$ where ϵ_{double} is the difference between one and the smallest IEEE double precision floating point number greater than one. Singular values less than ϵ are considered to be zero within working precision.

3.0.2 Implementation

A region is interpolated if and only if, when counting nodal domains, we encounter a point whose sign matches that of a point diagonally adjacent to it, but differs from the signs of the two points adjacent to both it and its diagonal

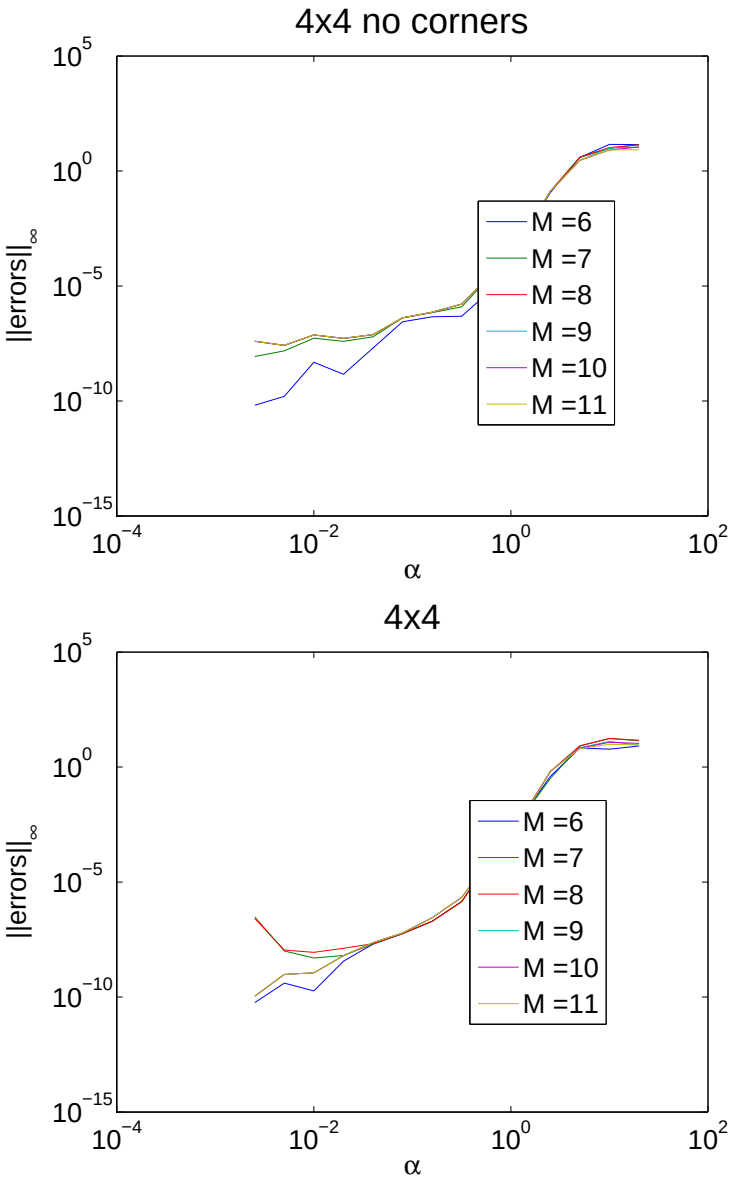

Figure 3.2: Comparison of interpolation error norms over M and α for each stencil.

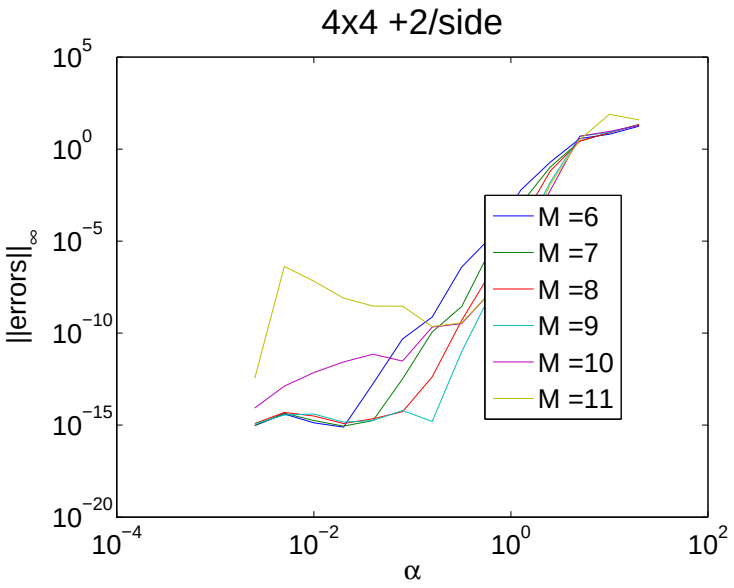
4x4 +2/side
10^{5}
10^{0}
10^{-5}
10^{-10}
10^{-15}
10^{-20}
$||errors||_{\infty}$
10^{-4}
10^{-2}
10^{0}
10^{2}
α
M =6
M =7
M =8
M =9
M =10
M =11

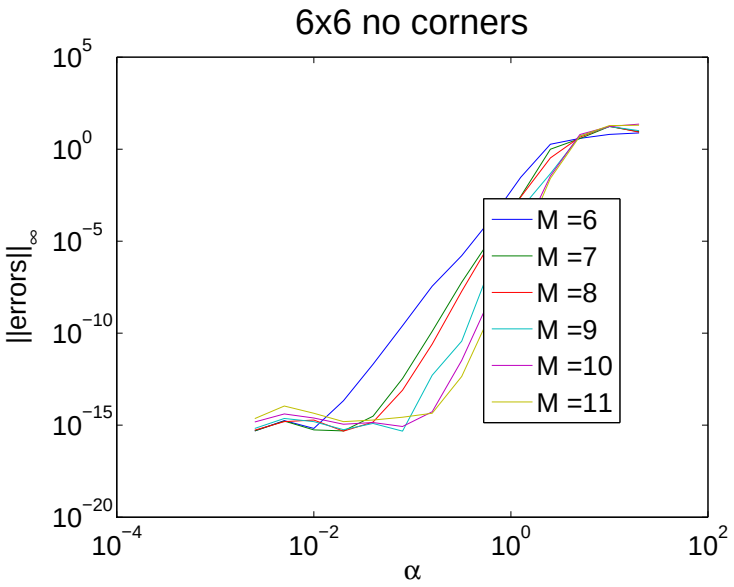
6x6 no corners
10^{5}
10^{0}
10^{-5}
10^{-10}
10^{-15}
10^{-20}
$||errors||_{\infty}$
10^{-4}
10^{-2}
10^{0}
10^{2}
α
M =6
M =7
M =8
M =9
M =10
M =11

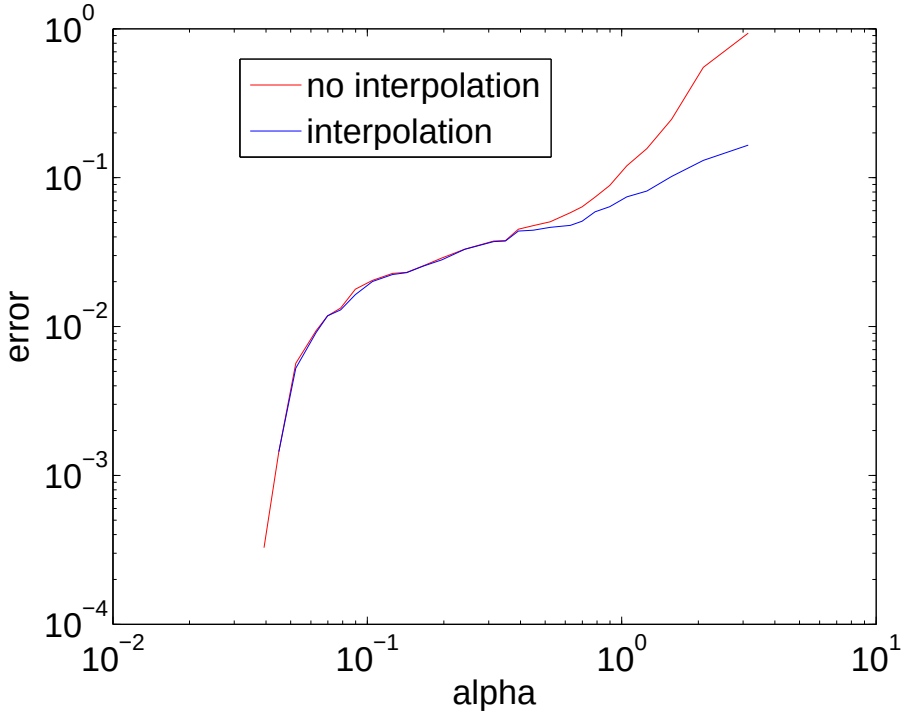

Figure 3.3: Error in nodal domain count for random plane waves

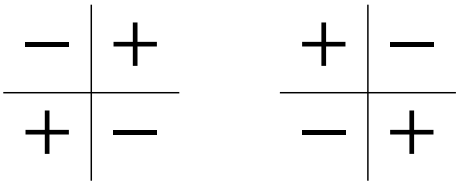

Figure 3.4: Configurations that will result in interpolation

neighbor (Fig. 3.4). In such a case we fill a vector $\mathbf{v}$ with the eigenfunction values at the stencil points surrounding the four points comprising the ambiguity. We then compute $\mathbf{w} = U\mathbf{v}$ where U is the interpolation matrix described above. This vector $\mathbf{w}$ contains estimated eigenfunction values with a spacing of $\frac{h}{\rho}$ between the four points comprising the ambigious region. We can use these values to determine the connectivity of the nodal domains by traversing pixel-by-pixel from the top-left pixel, in the same manner as above, until we either reach the bottom-right pixel or finish exploring the nodal domain. In the former case the nodal domain containing the top-left pixel connects to the nodal domain containing the bottom-right pixel and in the latter case the nodal domain containing the top-right pixel connects to the nodal domain containing the bottom-left pixel.

Code implementing Vergini's scaling method to compute eigenfunctions was written by Alex Barnett. Code for counting nodal domains was written by the author. All code used herein is open source and available under the GPL license [1] [6]. Appendix C contains an overview of the functions provided by this library.

3.1 Analysis

3.1.1 Probability of ambiguous region

Theory

Here we derive an upper bound on the probability of a trouble region using random plane waves. A random plane wave is simply a sum of plane waves travelling in all directions:

$$u(\mathbf{r}) = \Re \lim_{N\to\infty} \frac{1}{\sqrt{N}} \sum_{n=1}^{N} \omega_n \exp\{\mathrm{i}k\hat{n}_n \cdot \mathbf{r}\}$$

where $\omega_n \sim \mathcal{N}(0,1)$ are independent and identicially distributed and $\hat{n}_n = (\cos\frac{2\pi n}{N}, \sin\frac{2\pi n}{N})$. Applying the Jacobi-Anger expansion

$$\exp(\mathrm{i}kr\cos\theta) = \sum_{l\in\mathbb{Z}} \mathrm{i}^l \exp\{\mathrm{i}l\theta\} J_l(kr)$$

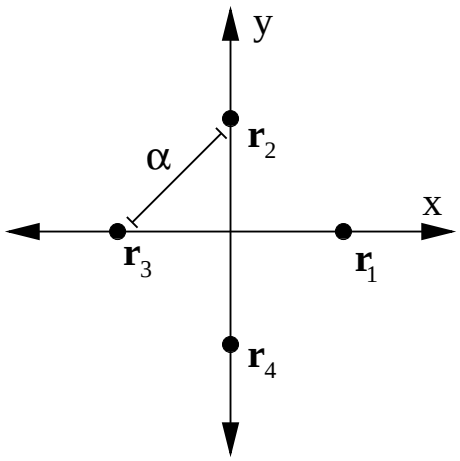

Figure 3.5: Four evaluation points in coordinate system

and the fact that $\hat{n}_n \cdot \mathbf{r} = r\cos\theta - \frac{2\pi n}{N}$ produces

$$u(\mathbf{r}) = \Re \sum_{l\in\mathbb{Z}} \mathrm{i}^l \tilde{\omega}_n \exp\{\mathrm{i}l\theta\} J_l(kr) \tag{3.1}$$

where $\mathbf{r} = (r, \theta)$ in polar coordinates and $\tilde{\omega}_n$ are given by

$$\tilde{\omega}_n = \lim_{N\to\infty} \frac{1}{\sqrt{N}} \sum_{n=1}^{N} \omega_n \mathrm{i}^l \exp\left\{-\mathrm{i}l\frac{2\pi n}{N}\right\}$$

Fixing N, we can express the transformation which takes ω_n to $\tilde{\omega}_n$ as a matrix

$$\overrightarrow{\tilde{\omega}}_n^{(N)} = A^{(N)} \overrightarrow{\omega}_n^{(N)}$$

where entries of $A^{(N)}$ are given by

$$a_{mn} = \frac{1}{\sqrt{N}} \mathrm{i}^m \exp\left\{-\mathrm{i}m\frac{2\pi n}{N}\right\} = \frac{1}{\sqrt{N}} \exp\left\{-\mathrm{i}m\left(\frac{2\pi n}{N} - \frac{\pi}{2}\right)\right\}$$

The operator A is simply a discrete fourier transform and therefore acts on $\omega n \sim \mathcal{N}(0,1)$ i.i.d. to produce $\tilde{\omega}_n \sim \mathcal{N}(0,1)$ i.i.d.

Expanding the first three terms of 3.1 gives

$$u(\mathbf{r}) = a_0 J_0(kr) + J_1(kr)(a_1\cos\theta + b_1\cos\theta) + J_2(kr)(a_2\cos\theta + b_2\cos\theta) + \dots$$

where $a_0 = \Re\tilde{\omega}_0$, $a_{1,2} = \Re\tilde{\omega_1} - \tilde{\omega_{-1}}$, and $b_{1,2} = \Im\tilde{\omega_1} - \tilde{\omega_{-1}}$. Note that $a_0 \sim \mathcal{N}(0,1)$ and $a_1, b_1, a_2 \sim \mathcal{N}(0,\sqrt{2})$

We now consider four points forming a square of side length α. We define a coordinate system with origin at the center of the square and axes rotated

such that each corner of the square falls on either the x- or y-axis (figure 3.5). We label the four points $\mathbf{r}_1$ through $\mathbf{r}_4$. Evaluating the three term expansion of $u(\mathbf{r})$ at the four points gives

$$\begin{aligned} u(\mathbf{r}_1) &= a_0\beta_0 + a_1\beta_1 + a_2\beta_2 \\ u(\mathbf{r}_2) &= a_0\beta_0 + b_1\beta_1 - a_2\beta_2 \\ u(\mathbf{r}_3) &= a_0\beta_0 - a_1\beta_1 + a_2\beta_2 \\ u(\mathbf{r}_4) &= a_0\beta_0 - b_1\beta_1 - a_2\beta_2 \end{aligned}$$

where $\beta_i = J_i\left(k\frac{\alpha}{\sqrt{2}}\right)$. Interpolation is required if $u(\mathbf{r}_1), u(\mathbf{r}_3) < 0$ and $u(\mathbf{r}_2), u(\mathbf{r}_4) > 0$ (or the reverse case) which gives the system of inequalities

$$\begin{aligned} a_0\beta_0 + a_1\beta_1 + a_2\beta_2 &< 0 \\ a_0\beta_0 + b_1\beta_1 - a_2\beta_2 &> 0 \\ a_0\beta_0 - a_1\beta_1 + a_2\beta_2 &< 0 \\ a_0\beta_0 - b_1\beta_1 - a_2\beta_2 &> 0 \end{aligned}$$

which gives the constraints

$$\begin{aligned} a_2 &< 0 \\ a_1 &< a_2\frac{\beta_2}{\beta_1} \\ a_0 &< a_2\frac{\beta_2}{\beta_0} \\ b_1 &< 2a_2\frac{\beta_2}{\beta_1} - a_1 \end{aligned}$$

Thus the probability of a configuration of four points requiring interpolation is given by

$$2\int_{-\infty}^{0}\int_{-\infty}^{a_2\frac{\beta_2}{\beta_1}}\int_{-\infty}^{2a_2\frac{\beta_2}{\beta_1}-a_1}\int_{-\infty}^{a_2\frac{\beta_2}{\beta_0}} f(a_0,a_1,b_1,a_2)\,\mathrm{d}a_0\,\mathrm{d}b_1\,\mathrm{d}a_1\,\mathrm{d}a_2 \qquad (3.2)$$

where the factor of two is inserted to account for the possibility of the inequalities being reversed and $f(a_0, a_1, b_1, a_2)$ is a four dimensional Gaussian distribution

$$f(a_0,a_1,b_1,a_2) = \frac{1}{(2\pi)^2|\Sigma|^{\frac{1}{2}}}\exp\left\{\mathbf{x}^T\Sigma^{-1}\mathbf{x}\right\}$$

where

$$\mathbf{x} = \begin{pmatrix} a_0 \\ a_1 \\ b_1 \\ a_2 \end{pmatrix} \qquad \Sigma = \begin{pmatrix} 1 & 0 & 0 & 0 \\ 0 & 2 & 0 & 0 \\ 0 & 0 & 2 & 0 \\ 0 & 0 & 0 & 2 \end{pmatrix}$$

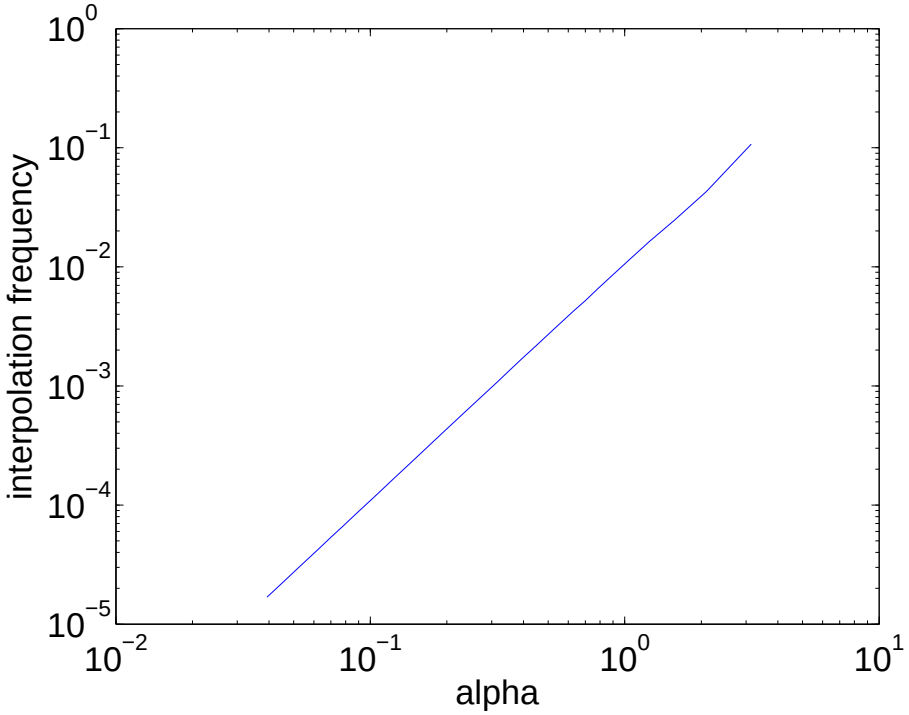

Figure 3.6: Mean number of interpolations per sample point on random plane waves. The number of interpolations scales like α^2.

giving

$$f(a_0, a_1, b_1, a_2) = \frac{1}{(2\pi)^2 2^{\frac{3}{2}}} \exp\left\{-\frac{1}{2}\left(a_0^2 + \frac{a_1^2}{2} + \frac{b_1^2}{2} + \frac{a_2^2}{2}\right)\right\}$$

The heuristic we use when deciding where to interpolate may miss some very rare cases where domains connect between sampled points. See [7] for a more complete characterization of sampling errors when computing nodal domains in two dimensions.

Empirical

Using random plane waves we can empirically compute the frequency of interpolation (fig. 3.6)

Chapter 4

Results

4.1 Data Collected

We computed approximately 100,000 eigenfunctions and counted 1.5 billion nodal domains. This data was collected over several weeks running on the Dartmouth Mathematics Condor cluster. Table 4.1 shows the number of eigenfunctions and nodal domains which were computed and counted in various k ranges.

4.2 Mean of number of nodal domains

We reject conjecture 1 for the both the Sinai and stadium billiards. In both cases, there is a slow convergence from above to a mean that differs from the predicted value 4.1. The rate of convergence (agrees/disagrees) with the percolation model.

4.3 Variance of number of nodal domains

The variance of number of nodal domains in quantum chaotic eigenfunctions does not agree with 2 for either billiard shape.

Billiard	k_{low}	k_{high}	Eigenfucntions	Nodal Domains	α	data size	CPU time
Sinai	1000	1200	2.11e4	3.97e8	0.5	385GB	TODO
Sinai	2000	2020	3.90e3	?	0.7	120GB	
Stadium	700	900	4.55e4	1.2e9	0.7	221GB	
Percolation	100	2000	3.18e4	9.07e6	N/A	N/A	

Table 4.1: Data collected

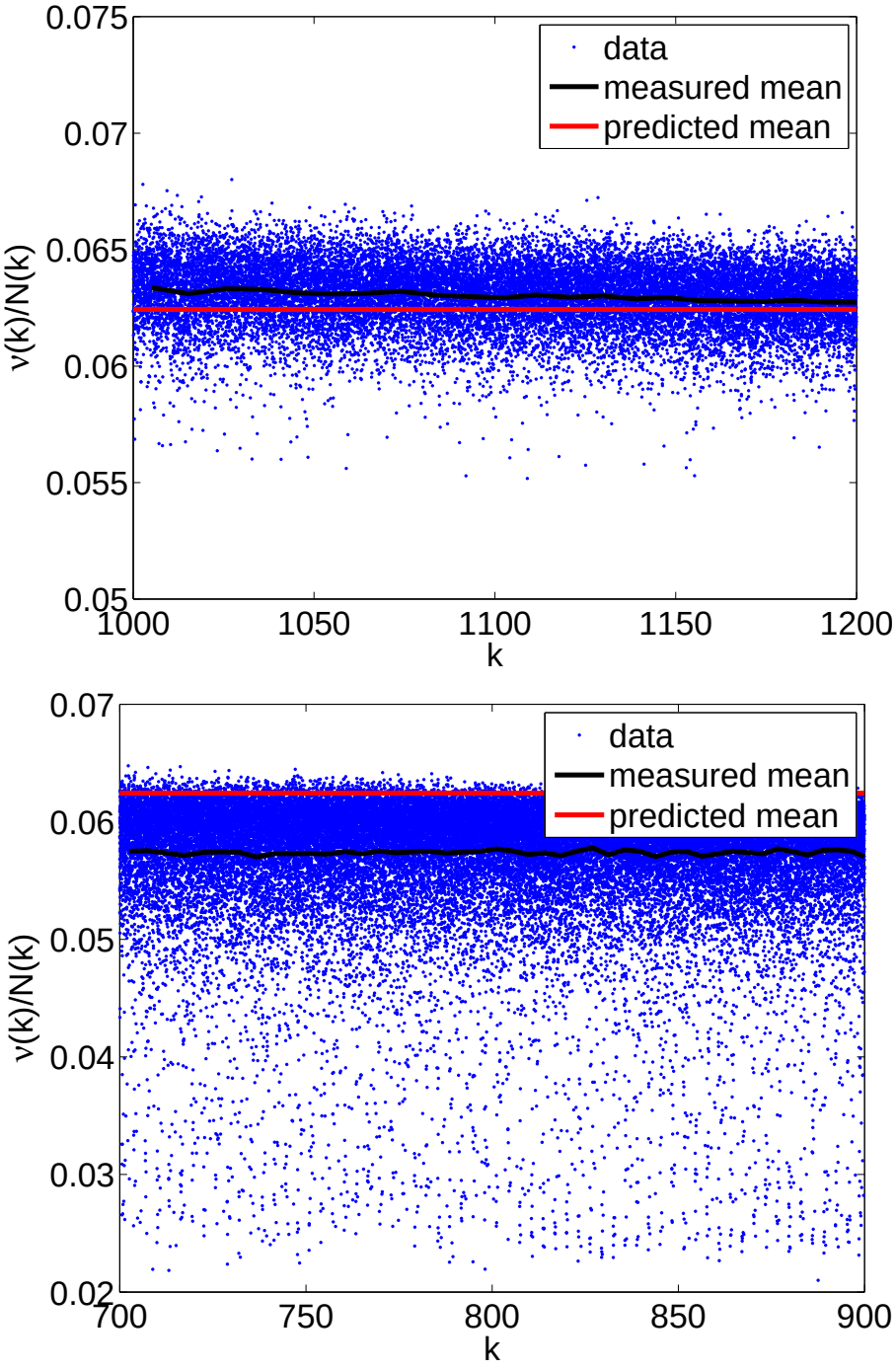

Figure 4.1: Mean number of nodal domains. Top: Sinai; middle: stadium; bottom: percolation

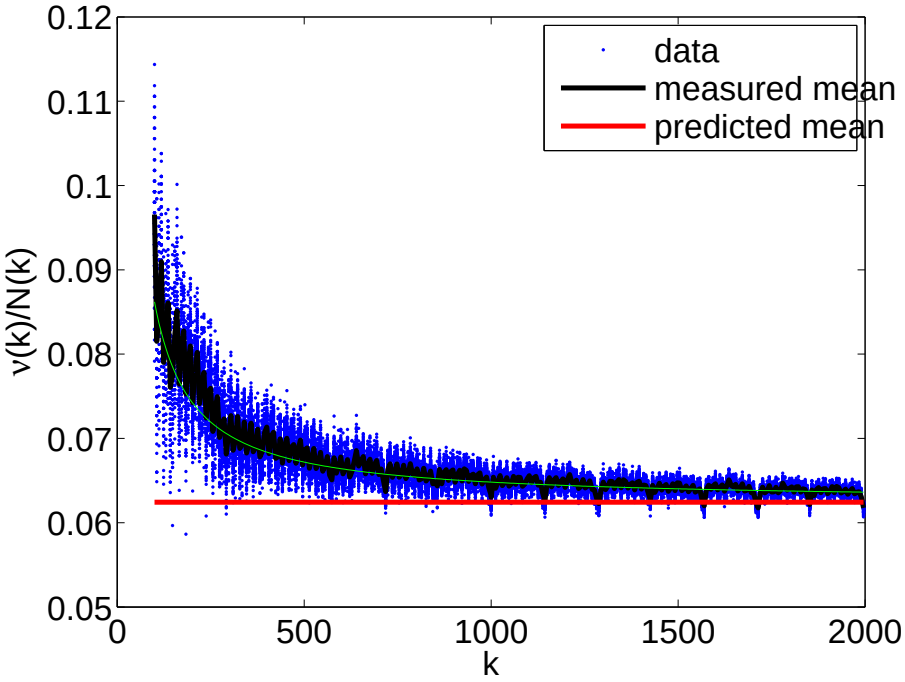

4.4 Areas of nodal domains

The distribution of area of nodal domains is slightly different. TODO: confidence that slopes differ

4.5 Interpolation frequency

At $\alpha = 0.5$ interpolation occured on average 0.1512 times per nodal domain and $1.9e-4$ times per pixel. At $\alpha = 0.7$ interpolation occured on average 0.3838 times per nodal domain and $9.1e-4$ times per pixel.

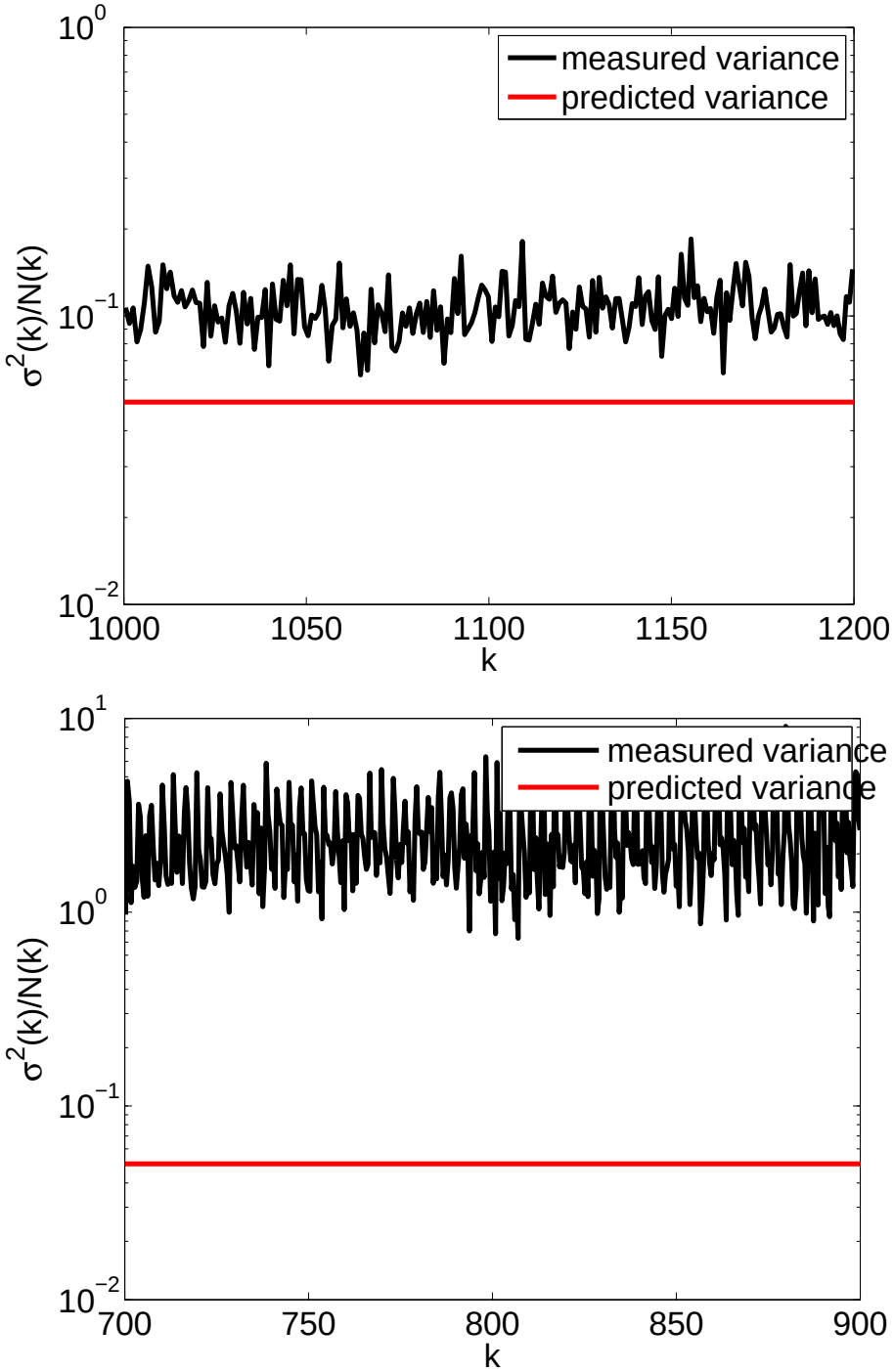

Figure 4.2: Variance of number of nodal domains. Top: Sinai; middle: stadium; bottom: percolation

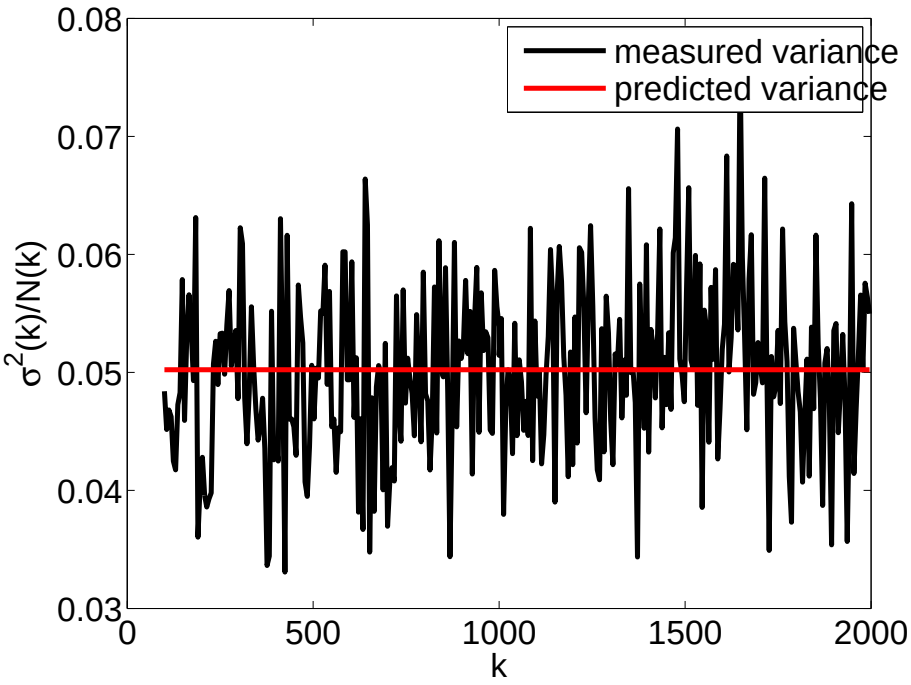
measured variance
predicted variance
0.08
0.07
0.06
0.05
0.04
0.03
σ2(k)/N(k)
0
500
1000
1500
2000
k

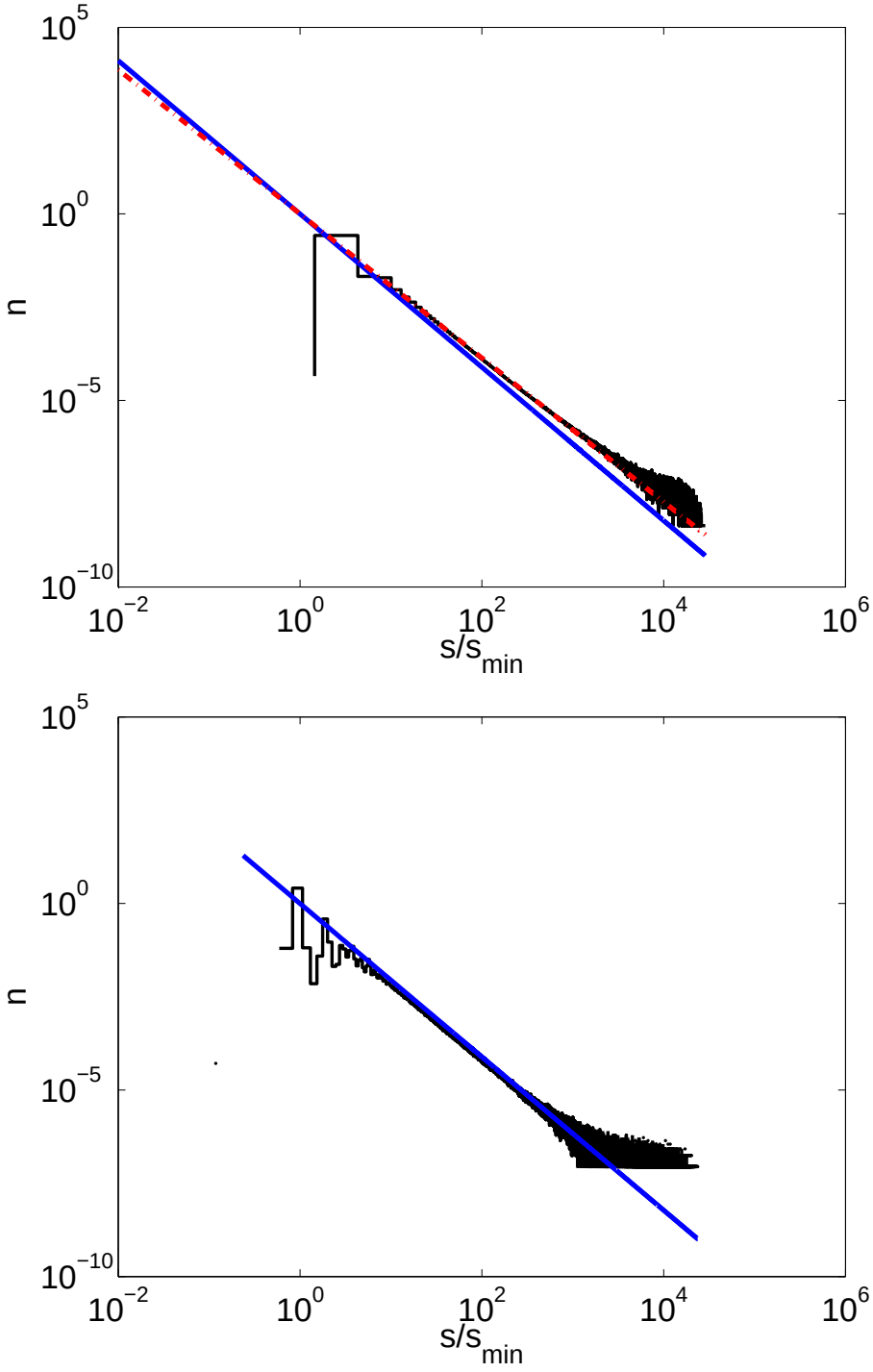

Figure 4.3: area of nodal domains. Above: Sinai; below: stadium

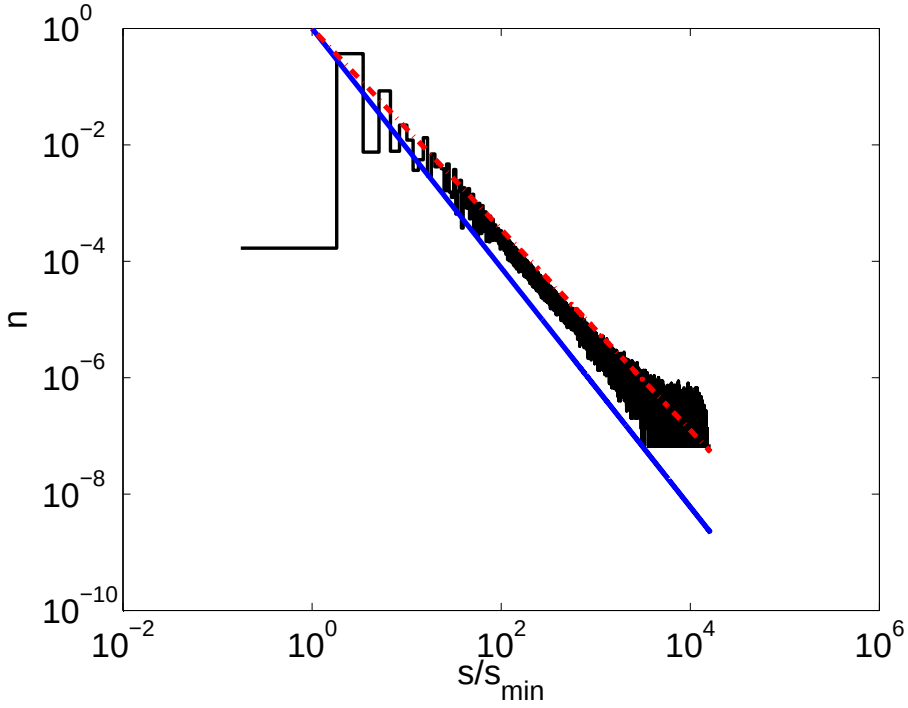
10^{0}
10^{-2}
10^{-4}
10^{-6}
10^{-8}
10^{-10}
n
10^{-2}
10^{0}
10^{2}
10^{4}
10^{6}
s/s_{min}

Chapter 5

Conclusion

By combining the scaling method of Vergini and Saraceno [8] with adaptive interpolation, we have obtained nodal domain data at energies much higher than any previous work. Comparing this data to the predictions of Bogomolny and Schmidt [4] from the percolation model, we find different values for the mean and variance of nodal domain counts as well as the distribution of sizes of nodal domains.

Appendix A

Definition of Ergodicity

Informally, a mapping T is said to be ergodic if it has homogenous dynamics across its domain, i.e., there are no regions which behave "differently" under the mapping T. Formally, we consider T as a mapping on a probability space. A probabilty space requires a measure, which is defined over a σ-algebra. Thus we present the following definitions:

Definition 1 (σ-algebra)**.** $\Sigma \subset 2^{\Omega}$ *is a* σ-algebra *over* Ω *if:*

1. $\emptyset, \Omega \in \Sigma$
2. $\Omega \backslash A \in \Sigma \; \forall A \in \Sigma$
3. $\cup_{i=1}^{\infty} A_i \in \Sigma \; \forall \, \{A_i\}_{i=1}^{\infty}$ *such that* $A_i \in \Sigma \forall i$

Definition 2 (Measure)**.** μ*:* $\Sigma \to \mathbb{R}$ *is a* measure *on* Σ *if:*

1. $\mu(A) \geq 0 \; \forall A \in \Sigma$
2. $\mu(\emptyset) = 0$
3. $$\mu\left(\cup_{i=1}^{\infty} A_i\right) = \sum_{i=1}^{\infty} \mu(A_i)$$

Definition 3 (Measure space)**.** *A* measure space *is a triple* (Ω, Σ, μ) *where* Σ *is a* σ*-algebra over* Ω *and* μ *is a measure on* Σ*.*

Definition 4 (Probability space)**.** *A* probability space *is a measure space* (Ω, Σ, μ) *where* $\mu(\Omega) = 1$*.*

These definitions allow us to formally define ergodicity as:

Definition 5 (Ergodicity)**.** *Let* (Ω, Σ, μ) *be a probability space. A mapping* T*:* $\Sigma \to \Sigma$ *is* ergodic *if* $T(E) = E \implies \mu(E) = 0$ *or* $\mu(E) = 1$

Thus, under an ergodic mapping T, any $E \in \Sigma$ that maps to itself must have measure zero (in which case dynamics on this set are inconsequential) or measure one (in which case the set is almost the entire domain Ω). Futhermore, all $E \in \Sigma$ such that $0 < \mu(E) < 1$ must contain points that map to points outside of E under T. In this sense, T "mixes" points in the domain Ω.

Appendix B

General Solution of the Helmholtz Equation

Here we show that the functions $J_n(kr)\sin(n\theta)$ and $J_n(kr)\cos(n\theta)$ form a complete orthonormal basis of solutions of (1.1).

In polar coordinates,

$$\Delta = \frac{1}{r}\partial_r(r\partial_r) + \frac{1}{r^2}\partial_{\theta\theta}$$

Thus, (1.1) can be expressed as

$$u_{rr}(r,\theta) + \frac{1}{r}u_r(r,\theta) + \frac{1}{r^2}u_{\theta\theta}(r,\theta) + k^2u(r,\theta) = 0$$

Using separation of variables we attempt solutions of the form

$$u(r,\theta) = R(r)\Theta(\theta)$$

where $\Theta(\theta)$ is periodic with period 2π. This gives

$$\Theta''(\theta) + n^2\Theta(\theta) = 0$$

and

$$r^2R''(r) + rR'(r) + r^2k^2R(r) - n^2R(r) = 0$$

The periodicity of $\Theta(\theta)$ requires that

$$\Theta(\theta) = \alpha\sin(n\theta) + \beta\cos(n\theta)$$

where $n \in \mathbb{Z}$. The radial differential equation is known as Bessel's equation and has solutions

$$R(r) = J_n(kr)$$

where J_n is a regular Bessel function and $k \in \mathbb{R}$ is allowed to take discrete values determined by boundary conditions.

Thus, the general solution of (1.1) can be expressed as a sum of the form

$$b_0 J_0(kr) + \sum_{n=1}^{\infty} a_n J_n(kr) \sin n\theta + b_n J_n kr \cos n\theta \tag{B.1}$$

Appendix C

Code Interface

C.1 Command Line Interface

C.1.1 Verg

The verg program uses the scaling method described in 2.1 to find eigenvalues and eigenfunctions of the Laplace operator on domains in $\mathbb{R}^2$.

```
verg -l qust:2 -b 10 -s vepwoo:1.2:40:1.5 -k 200.01 -V 0.005 -f 0.001 -m
verg -l qugrs:1:0.4:0.7 -s oyooo:1.5:7:1 -u -4 1 -k 200.1 -V 0.005 -f 0.001 -m
```

C.1.2 Count

```
count -f t.sta_bin -m t.mask.sta_bin -l qust:2 -d .001 -k 200.01 -M 8 -u 20
```

The count program counts nodal domains over a domain in $\mathbb{R}^2$ using the adaptive interpolation scheme described in 2.3.

C.1.3 Vc

```
vc -n run_2018.450000 -l qugrs:1.0:0.4:0.7 -s oyooo:1.5:7:1 -u -4 1 -k 2018.450000 -V 0.0500
```

The vc program combines verg and count to compute eigenfunctions and count their nodal domains.

C.1.4 Perc

```
perc -r 100:6:1000 -N 100
```

The perc program generates random grids using the percolation model described in 1.4 and counts the nodal domains in the generated grids.

Bibliography

[1] Gnu general public license. `http://www.gnu.org/licenses/gpl.html`.

[2] A. Barnett. Asymptotic rate of quantum ergodicity in chaotic euclidean billiards. *Communications in Pure and Applied Mathematics*, 59(10):1457–1488, 2006.

[3] A. Barnett and A. Hassell. Fast computation of high frequency dirichlet eigenmodes via the spectral flow of the interior neumann-to-dirichlet map. 2012.

[4] E. Bogomolny and C. Schmit. Percolation model for nodal domains of chaotic wavefunctions. *Physical Review Letters*, 88(11), 2002.

[5] P. R. Garabedian. *Partial differential equations*. John Wiley & Sons Inc., New York, 1964.

[6] Kyle Konrad. qc. `https://github.com/ktkonrad/qc`.

[7] K. Mischaikow and T. Wanner. Probabalistic validation of homology computation for nodal domains. *The Annals of Applied Probability*, 17(3):980–1018, 2007.

[8] E. Vergini. Calculation by scaling of highly excited states of billiards. *Physical Review E*, (3):2204–2207, 1995.

[9] I. Wigman. On the nodal line of random and deterministic laplace eigenfunctions. 2011.